

Lithium in M67: from the main sequence to the red giant branch

Giancarlo Pace¹, Matthieu Castro², Jorge Meléndez³, Sylvie Théado⁴ and José-Dias do Nascimento Jr.²

¹ Centro de Astrofísica, Universidade do Porto, Rua das Estrelas, 4150-762 Porto, Portugal

² Departamento de Física Teórica e Experimental, Universidade Federal do Rio Grande do Norte, CEP: 59072-970 Natal, RN, Brazil

³ Departamento de Astronomia do IAG/USP, Universidade de São Paulo, Rua do Matão 1226, São Paulo, 05508-900, SP, Brazil

⁴ Laboratoire d'Astrophysique de Toulouse-Tarbes, Observatoire Midi-Pyrénées, 31400 Toulouse, France

Received : Accepted

ABSTRACT

Context. Lithium abundances in open clusters are a very effective probe of mixing processes, and their study can help to understand the large depletion of lithium in the Sun. Due to its age and metallicity, the open cluster M67 is especially interesting on this regard. Many studies on lithium abundances in M67 have already been performed, but a homogeneous global analysis of lithium in stars from subsolar up to the most massive members, was never accomplished for a large sample based on high-quality spectra.

Aims. We tested our non-standard models, which were calibrated using the Sun with observational data.

Methods. We collected literature data to follow, for the first time in a homogeneous way, NLTE lithium abundances of all observed single stars in M67 more massive than $\sim 0.9 M_{\odot}$. Our grid of evolutionary models were computed with non-standard mixing at metallicity $[\text{Fe}/\text{H}] = 0.01$, using the Toulouse-Geneva evolution code. The analysis is started from the entrance in the ZAMS.

Results. Lithium in M67 is a tight function of mass for stars more massive than the Sun, apart of a few outliers. A plateau in lithium abundances is observed for turn-off stars. Both less massive ($M \leq 1.10 M_{\odot}$) and more massive ($M \geq 1.28 M_{\odot}$) stars are more depleted than those in the plateau. There is a significant scatter in lithium abundances for any given mass lower than $M \leq 1.1 M_{\odot}$.

Conclusions. Our models qualitatively reproduce most of the features described above, although the predicted depletion of lithium is 0.45 dex smaller than observed for masses in the plateau region, i.e. between 1.1 and 1.28 solar masses. Clearly, more work is needed to thoroughly match the observations. Despite hints that chromospheric activity and rotation play a role in lithium depletion, no firm conclusion can be drawn with the presently available data.

Key words. Stars: fundamental parameters – Stars: abundances – Stars: evolution – Stars: interiors – Stars: solar-type

1. Introduction

Lithium is destroyed by proton capture at temperatures above 2.4×10^6 K. In Sun-like stars, material in layers at this temperature can be mixed with photospheric layers through convection and diverse processes such as diffusion, meridional circulation and internal gravity waves (e.g. Talon 2008). As a consequence, stars undergoing such processes have lower lithium abundances than their initial value. This phenomenon is known as lithium depletion, and makes lithium abundance one of the most effective probes of mixing processes in stars.

Astronomers have long dedicated huge observational and theoretical efforts to understand how and when lithium is depleted in stars. Depletion of lithium can occur both during the pre-main sequence and during the main sequence lifetime of solar type stars (e.g. D'Antona & Mazzitelli 1984, 1994; D'Antona & Montalbán 2003; Boesgaard & Budge 1988; Pinsonneault et al. 1989; Hobbs et al. 1989; Charbonnel et al. 1992; Pasquini et al. 1994; Chaboyer et al. 1995; Ventura et al. 1998; Montalbán & Schatzman 1996; Chen et al. 2001; Piau & Turck-Chièze 2002; Théado & Vauclair 2003b; Lambert & Reddy 2004; Takeda & Kawonomoto 2005; Sestito & Randich 2005; Sestito et al. 2006). Lithium depletion by rotationally-driven mixing has been related to the rotational history of stars, which, in turn, has been related to planet formation (e.g. Bouvier 2008). Indeed, the influence of planets is the subject of a hot debate. There are claims

of stronger lithium depletion in planet hosting stars but only in a very narrow range around solar T_{eff} (Gonzalez 2008; Israelian et al. 2009). However, such evidence has been challenged by other authors, who claim that no difference in lithium abundance is detected between stars with and without detected planets when unbiased samples are analyzed (Meléndez et al. 2010; Ghezzi et al. 2010; Baumann et al. 2010). Furthermore, at a given mass and metallicity there is a clear relation between lithium abundances and age, independently of the star being a planet host or not (Meléndez et al. 2010; Baumann et al. 2010).

Obviously, there are two main parameters favoring lithium depletion: how deep, i.e. how hot, the mixing reaches down; and how long the process has been active, i.e. the age of the star. However, the dependence of the former parameter on stellar mass, age, and metallicity is not simple, neither is there general consensus on what other parameters are involved, and, despite decades of observations in clusters and field stars, no clear and widely-accepted picture has been drawn yet.

Lithium abundance in open clusters is a precious tool to understand mixing processes because stars in open clusters share the same age and initial chemical composition, therefore allowing us to see how lithium depletion varies with stellar mass and to test non-standard models of stellar mixing. A crucial question, on which observation in clusters can cast light, is whether or not there is spread in lithium abundances for stars with the same fundamental parameters, i.e. mass, chemical composition, and age, which is to say, whether or not lithium abundance in a given open cluster is a tight function of the stellar mass. In case it is not, careful study of the deviating stars would be im-

Send offprint requests to: G. Pace, email: gpace@astro.up.pt

portant to constrain the parameters that are causing the spread of lithium abundances, such as for example the initial rotation velocity (Charbonnel & Talon 2005).

Some early observations indicated the presence of a certain amount of spread in the lithium abundances versus mass distribution in a few clusters, and its absence, or at least the lack of evidence for it, in many others. Examples of clusters belonging to the former group are the Pleiades (Duncan & Jones 1983; Soderblom et al. 1993a) and Praesepe (Soderblom et al. 1993b) for low mass stars ($M \leq 0.9 M_{\odot}$). However, many of the early claims about spread in the lithium versus mass distribution in open clusters have been lately revised. Xiong & Deng (2005, 2006) found that most, if not all, of the lithium dispersion for a given mass in members of α_{turb} Per and Pleiades, can be accounted for by inhomogeneous reddening, stellar spots and stellar surface activity, rather than by a genuine variation. King et al. (2000), analyzing Praesepe stars, ascribed most of the scatter to variations in activity-regulated ionization of the lithium atom. In support of this hypothesis, they mentioned the lesser amount of scatter in two older and chromospherically quieter open clusters: Hyades (Thorburn et al. 1993) and M34 (Jones et al. 1997). Now, we can add to the list several clusters older than the Hyades, such as NGC 752 (Sestito et al. 2004), NGC 188 (Randich et al. 2003), Berkeley 32 (Randich et al. 2009). There are, however, examples of old clusters presenting a significant amount of scatter. One of them is NGC 3680, but the scatter in this cluster is especially at temperatures higher than ~ 6500 K (Anthony-Twarog et al. 2009), and too few stars at lower temperature were analyzed. Another old cluster apparently showing spread in the lithium abundance distribution is M67, which is a well-studied cluster, subject to a number of lithium abundance investigations. However, a comprehensive study in which lithium abundances were analyzed for a large number of members in all evolutionary stages, taking advantage of already available high S/N spectra, was still lacking.

Since M67 has an age of about 3.9 Gyr (e.g. VandenBerg et al. 2007; Castro et al. 2011) and about solar metallicity (e.g. Tautvaišienė et al. 2000; Randich et al. 2006; Pace et al. 2008; Pasquini et al. 2008; Önehag et al. 2011), it can give us insight on the behavior of lithium in relatively old solar type stars, which is important to assess why some old solar analogs in the field seem to have too much lithium for their ages (Baumann et al. 2010).

In this work we homogenize all previous studies on M67 stars by obtaining a consistent set of temperatures, and by applying corrections to the lithium abundances when needed (due to revised effective temperatures) and taking into account non-LTE effects on the lithium abundances. We analyze stars from the main sequence to the red giant branch, comparing our models to the observed behavior of lithium abundance as a function of mass. In Sect. 2, we describe the data. In Sect. 3, we compare the effective temperatures from different references used in the paper. In Sect. 4, we present details of our stellar models, and in Sect. 5 we discuss our results. Finally, in Sect. 6 we give our conclusions.

2. Sample and data

Our database is a compilation of literature sources of lithium abundance measurements, namely: Canto Martins et al. (2011); Castro et al. (2011); Pasquini et al. (2008); Randich et al. (2007); Jones et al. (1999); Balachandran (1995). When multiple measurements were available for a single object, we adopted the most recent. Actually, some of the data included in our

compilation, namely data from Castro et al. (2011) and Table 2 in Jones et al. (1999), are refinement of previous abundance determinations. The final sample amounts to 103 stars. For the solar twin YBP 1194, Önehag et al. (2011) used the best spectra available to date to determine its lithium abundance, yet their result is essentially identical with that of Castro et al. (2011), which is based on lower quality spectra; thus, either of the sources can be adopted for the lithium abundance of YBP 1194. The data in Pasquini et al. (1997), Garcia Lopez et al. (1988), Spite et al. (1987), and Hobbs & Pilachowski (1986) were initially considered for the present compilation but eventually not used, since their whole sample was later re-analyzed in some of the works cited above. Neither we included in our compilation data from Deliyannis et al. (1994), which is a study on tidally locked binaries, whose mechanism of lithium depletion may be completely different from that of single stars.

In some works, no quantitative estimations of the error in the lithium abundances were given. All these cases are discussed below. Pasquini et al. (2008) stated that all the stars with upper limits in their sample may have a lithium abundance comparable to the solar one. Following this piece of information, we raised their upper limits (which in some cases were as low as 0.5 dex) to 1.0 dex, which is more reasonable considering the quality of the spectra available to Pasquini et al. (2008). However, this correction hardly changes the general picture drawn using data in Table A.2 of Pasquini et al. (2008), which points to a significant spread in lithium abundances at about one solar mass. Their estimation of the uncertainty in lithium abundance due to the uncertainty in the equivalent width, for a star with $A(\text{Li}) = 2.2$, is of ± 0.04 dex, and no evaluation is given for stars with lower abundances. Since lithium abundance is extremely sensitive to temperature, the uncertainty of the latter may contribute to that of the former in a non negligible way, even when it is extremely low. Such contribution was not quantified by Pasquini et al. (2008). Castro et al. (2011), in re-analyzing the solar twins of Pasquini et al. (2008) with spectral synthesis, find a global error of 0.1 dex. Their stars have Li abundances lower than the average of the sample studied by Pasquini et al. (2008). We conservatively assumed this error (0.1 dex) for all stars in Pasquini et al. (2008).

Jones et al. (1999) estimated an error of 0.05 dex in lithium abundance due to the uncertainty in the equivalent width, and an equal error due to the uncertainty in the temperature of 50 K. We were conservative once again, and we summed linearly these two sources of error and assumed for all lithium abundances an uncertainty of 0.1 dex. This same value was also assumed for their measurements made by re-analyzing literature data.

Information on photometry and membership was taken, whenever possible, i.e. for 95 out of 103 stars, from the work of Yadav et al. (2008), otherwise it was taken from the reference of the study on lithium abundance. Of the 95 stars of our sample studied by Yadav et al. (2008), 87 had radial velocity from the same source. For the remaining 8 stars, Yadav et al.'s membership information was based on photometry and proper motion. 6 out of the 8 stars of the final sample not studied by Yadav et al. (2008), have radial velocity available from the lithium abundance study, therefore, this piece of information, is only lacking for ten stars. We discarded stars with radial velocities out of the range of values from 30 to 38 km s^{-1} and we removed from our sample the blue stragglers Sanders 2204 and Sanders 997 and other known binaries.

In Fig. 1, we plot a color-magnitude diagram of M67 stars, and the isochrone calculated from our models, with the parameters for M67 found in Castro et al. (2011), i.e. $[\text{Fe}/\text{H}] = 0.01$,

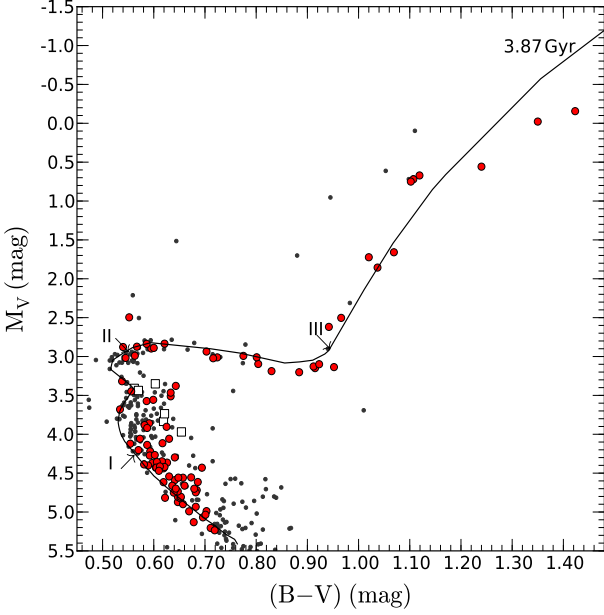


Fig. 1. Color-magnitude diagram for M67 superposed upon isochrone. The continuous isochrone corresponds to an age of 3.87 Gyr. The red filled circles represent our work sample, i.e. stars with lithium abundance measurements. Stars with photometry available from Yadav et al. (2008), but with no lithium abundances, are displayed, for comparison with the isochrone, as black points. The squares represent the deviant stars. The roman numbers I, II and III are described on the section 5.1 and they correspond to the temperatures of, respectively, 6095, 6123, and 4966 K.

$(m - M) = 9.68$, and $E(B - V) = 0.02$, and age of 3.87 Gyr. Black dots are the stars from the sample of Yadav et al. (2008), red filled circles are the stars studied in this paper, and open squares are deviant stars (see Sect. 5.3). Roman numbers I, II and III are defined in Sect. 5.

Photometric and membership information, are available at CDS in electronic form (Table 1).

3. Temperatures and corrected lithium abundances

Lithium abundances are strongly sensitive to the effective temperature. To check for the dependence on the adopted effective temperatures, we compared different estimates, using the literature source from which the lithium abundances were also taken, a photometric calibration, and the isochrone. To determine the effective temperature by means of the isochrone, we proceeded in the following way: we plotted in the same CMD data-points for each star and the isochrone computed for M67 age and metallicity, shifted according to its distance modulus and reddening. Then, for each stellar data-point, we took the closest point on the isochrone, and adopted the corresponding physical parameters, i.e., in the case under consideration, effective temperature. For the remainder of the paper, we will refer to this kind of temperature estimation either as “isochrone temperature”, or as T_{iso} with the possible further specification of the isochrone used. “Isochrone masses” were computed in the very same way. Summarizing, we have the following 4 temperature estimations:

1. the T_{eff} adopted in the paper from which the lithium abundance was taken (T_{orig});

2. the isochrone temperature adopting models and parameters for M67 as in Yadav et al. (2008), who in turn adopted BaSTI models (Pietrinferni et al. 2004) ($T_{\text{iso-BaSTI}}$);
3. the isochrone temperature adopting isochrone and parameters for M67 in Castro et al. (2011) ($T_{\text{iso-Castro}}$);
4. using a photometric calibration, from Casagrande et al. (2010) for dwarfs and sub-giants, and from Kučinskas et al. (2005) for giants (T_{calib} or “calibration temperature”).

A comparison between the different temperature evaluations shows that the differences are significant. When comparing T_{orig} with the other temperature evaluations, the heterogeneity of the data, especially in the assumed reddening for M67, is certainly a main cause for such differences, and one of the aims of the present study is to homogenize the different determinations. The mean differences between T_{orig} on one side, and $T_{\text{iso-BaSTI}}$, $T_{\text{iso-Castro}}$, and T_{calib} on the other, are, respectively, of 19, 50 and 95 K. The differences between calibration and isochrone temperatures arise, instead, from the fact that the isochrone in the CMD diagram leave most of the points on the right (cooler) side. This is due to the fact that calibration temperature is affected by the presence of undetected companions, which move the data points brighter and cooler in the CMD. In computing isochrone temperatures, we exploit the fact that the stars belong to the same cluster. In fact, the isochrone on the CMD is the locus where we expect all the photometric datapoints to be if there were no photometric errors and no multiple systems. T_{iso} is the temperature corresponding to such locus, therefore, it should not be affected by the presence of undetected companions. This is confirmed by the overall good agreement between T_{iso} and T_{orig} for the 82 stars studied in Canto Martins et al. (2011), Castro et al. (2011), and Pasquini et al. (2008). In these stars, T_{orig} is based on spectroscopic analysis and is therefore very precise. Let us label T_{spec} this subset of T_{orig} based on spectroscopic analysis. The linear best fit to the data-points in the T_{spec} versus isochrone temperature graph is very close to identity: $T_{\text{iso-BaSTI}} = 0.99 \cdot T_{\text{spec}} - 2.5$ K. We can confidently claim that the errors on isochrone temperatures are random in nature.

We note that the two different evaluation of effective temperature using either isochrone, i.e. $T_{\text{iso-BaSTI}}$ and $T_{\text{iso-Castro}}$, are consistent with each other within the margins of error for most of the stars. The only significant differences arise for sub-giant stars and, to a lesser extent, for turn-off stars.

Corrections to lithium abundance measurements were applied according to the differences between T_{orig} and, respectively, $T_{\text{iso-BaSTI}}$, $T_{\text{iso-Castro}}$, and T_{calib} . At the same time, we also took into account NLTE effects using the grid of NLTE corrections computed by Lind et al. (2009).

All temperature estimations, corrected and uncorrected lithium abundances, along with the photometric and membership information, are available on-line in Table 1.

In Fig. 2 we plotted the lithium abundances as a function of mass for both the stellar data-points and two models. Red filled circles with error bars are the stars of our sample with detected lithium line, green filled triangles represent upper limits. Open squares with error bars and, only in the case of one upper limit, the open triangle, represent the deviant stars discussed in Sect. 5.3. The models will be discussed extensively in Sect. 4.

As mentioned above, Canto Martins et al. (2011); Castro et al. (2011); Pasquini et al. (2008) computed temperature by carrying out detailed spectroscopic analysis. Their temperature evaluation is more precise than that obtained using photometric information. Therefore, for the 82 stars studied in

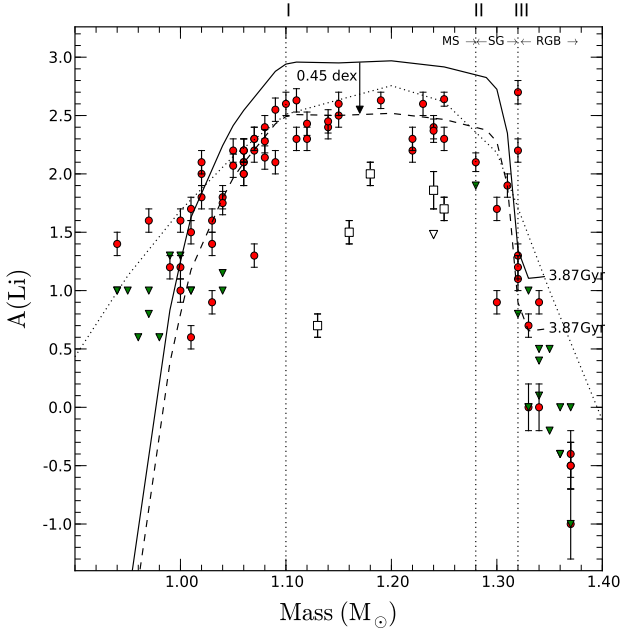


Fig. 2. Lithium abundances as a function of stellar mass determined from the isochrone. Red filled circles represent stars with lithium abundance redetermined. The green triangles represent the lithium abundance upper limits. The open squares represent the deviant stars as discussed in the Sect. 5.3. Continuous line corresponds to the lithium abundance predicted by our models with rotation-induced mixing calibrated on the Sun at the age of M67. The dashed line represents the same model shifted by 0.45 dex to match the observed lithium plateau. The dotted line represents models with rotation-induced mixing calibrated on the Hyades. The roman numbers I, II and III are described on the section 5.1.

these works, we used the values given in the literature to do Fig. 2. On the contrary, for the remaining 21 stars, we used $T_{\text{iso-Castro}}$, and the corresponding corrected value of the lithium abundance. For all of the stars, the mass adopted is the isochrone mass, computed using the isochrone and the parameters for M67 adopted in Castro et al. (2011).

4. Stellar evolutionary models

For this study, stellar evolutionary models were computed using the Toulouse-Genève stellar evolution code TGEC (Hui-Bon-Hoa 2008). Details on the physics of these models can be found in Richard et al. (1996, 2004), do Nascimento et al. (2000), and Hui-Bon-Hoa (2008).

4.1. Input physics

We used the OPAL2001 equation of state by Rogers & Nayfonov (2002) and the radiative opacities by Iglesias & Rogers (1996), completed with the low temperature atomic and molecular opacities by Alexander & Ferguson (1994). The nuclear reactions are from the analytical formulae of the NACRE (Angulo et al. 1999) compilation, taking into account the three pp chains and the CNO tricycle with the Bahcall & Pinsonneault (1992) screening routine. Convection is treated according to the Böhm-Vitense (1958) formalism of the mixing length theory with a mixing length parameter

$\alpha = l/H_p = 1.74$, where l is the mixing length and H_p the pressure height scale. For the atmosphere, we use a gray atmosphere following the Eddington relation, which is a good approximation for main-sequence solar-type stars (VandenBerg et al. 2008).

The abundance variations in the following chemical species are computed individually in the stellar evolution code: H, He, C, N, O, Ne, and Mg. Both Li and Be are treated separately only as a fraction of the initial abundance. The heavier elements are gathered in a mean species Z. The initial composition follows the Grevesse & Noels (1993) mixture with an initial helium abundance $Y_{\text{ini}} = 0.268$. We chose to use the “old” abundances of Grevesse & Noels (1993) instead of the “new” mixture of Asplund et al. (2009). This choice is motivated by the disagreement between models computed with the new abundances and the helioseismic inversions for the sound-speed profile, the surface helium abundance, and the convective zone depth (e.g. Serenelli et al. 2009). Furthermore, according to Caffau et al. (2009), the solar metallicity using their own 3D analysis is $Z = 0.0156$ and $Z/X = 0.0213$, which are closer to those of Grevesse & Noels (1993). Anyway, the issue of the solar abundances is certainly still open and at present it is not clear yet whether the problem is due to the solar model or to the new low solar abundances. Notice that accretion of metal-poor material (e.g. Castro et al. 2007; Guzik & Musack 2010) recently supported by the lack of refractory elements in the solar atmosphere (Meléndez et al. 2009), may help to reduce the discrepancy between the solar model and helioseismic data. Thus, the low solar abundances of Asplund et al. (2009) may actually be representative of the solar photosphere while in the solar interior the abundances may be higher.

Diffusion and rotation-induced mixing.

The microscopic diffusion is computed with the atom test approximation. All models include gravitational settling with diffusion coefficients computed as in Paquette et al. (1986). Radiative accelerations are not computed here, since we focus only on solar-type stars where their effects are small when mixing is taken into account (Turcotte et al. 1998; Delahaye & Pinsonneault 2005). Rotation-induced mixing is computed as described in Théado & Vauclair (2003a). This prescription is an extension of the approach of Zahn (1992) and Maeder & Zahn (1998), and introduces the feedback effect of the μ -currents in the meridional circulation, caused by the diffusion-induced molecular weight gradients. It introduces two free parameters in the computations: C_h and α_{turb} (cf. Eq. (20) of Théado & Vauclair 2003a). The evolution in the rotation profile follows the Skumanich’s law (Skumanich 1972) with an initial surface rotation velocity on the ZAMS equal to $V_i = 100 \text{ km.s}^{-1}$, which roughly corresponds to the mean rotation velocity of stars hotter than about 7000 K in the Hyades according to the statistical study of Gaige (1993). The parameters of the Skumanich’s law are calibrated to match the solar rotation velocity at the solar age ($\sim 2 \text{ km.s}^{-1}$). Other prescriptions were tested by other authors to model the lithium destruction. Charbonnel & Talon (1999) and Palacios et al. (2003) included angular momentum transport induced by mixing. However, since a rotation-induced mixing alone cannot account for the flat rotation profile inside the Sun, these authors later introduced the possible effect of internal gravity waves triggered at the bottom of the convective zone (see e.g. Talon & Charbonnel 2005), which allows to reproduce the hot side of the Li-dip. Other authors suggested that the internal magnetic field is more important than internal waves in transporting angular momentum (Gough & McIntyre 1998). In any case, when applied to the solar case, all of these

prescriptions are able to reproduce the lithium depletion observed in the Hyades, and the results are ultimately quite similar (Talon & Charbonnel 1998; Théado & Vauclair 2003b).

We also include a shear layer below the convective zone, which is treated as a tachocline (see Spiegel & Zahn 1992). This layer is parametrized with an effective diffusion coefficient that decreases exponentially downwards (Brun et al. 1998, 1999; Richard et al. 2004):

$$D_{\text{tacho}} = D_{\text{bcz}} \exp\left(\ln 2 \frac{r - r_{\text{bcz}}}{\Delta}\right)$$

where D_{bcz} and r_{bcz} are the value of D_{tacho} at the bottom of the convective zone and the radius at this location respectively, and Δ is the half width of the tachocline. Both D_{bcz} and Δ are free parameters and the absolute size of the tachocline (i.e., Δ/R_* where R_* is the radius of the star) is supposed to be constant during the evolution. An overshooting of parameter $\alpha_{\text{ov}} = 0.01H_p$ has been included in the models which develop a convective core.

4.2. Models and calibration

We calibrated a model of $1.00 M_{\odot}$ to match the observed solar effective temperature and luminosity at the solar age. The calibration method of the models is based on the Richard et al. (1996) prescription: for a $1.00 M_{\odot}$ star, we adjusted the mixing-length parameter α and the initial helium abundance Y_{ini} to reproduce the observed solar luminosity and radius at the solar age. The observed values that we used are those of Richard et al. (2004), i.e., $L_{\odot} = 3.8515 \pm 0.0055 \times 10^{33} \text{ erg.s}^{-1}$, $R_{\odot} = 6.95749 \pm 0.00241 \times 10^{10} \text{ cm}$, and $t_{\odot} = 4.57 \pm 0.02 \text{ Gyr}$. For the best-fit solar model, we obtained $L = 3.8501 \times 10^{33} \text{ erg.s}^{-1}$ and $R = 6.95524 \times 10^{10} \text{ cm}$ at an age $t = 4.576 \text{ Gyr}$.

The free parameters of the rotation-induced mixing determine the efficiency of the turbulent motions. They are adjusted to produce a mixing that is both: 1) efficient and deep enough to smooth the diffusion-induced helium gradient below the surface convective zone, thus improving the agreement between the model and seismic sound speed profiles; 2) weak and shallow enough to avoid the destruction of Be. Following Grevesse & Sauval (1998), the Be abundance of the Sun is $A(\text{Be}) = 1.40 \pm 0.09$. We obtained a slight Be destruction by a factor of 1.33 with respect to the meteoritic value, which is well within the error in the determination of the solar Be abundance.

The calibration of the tachocline allows us to reach the solar lithium depletion ($A(\text{Li}) = 1.10 \pm 0.10$ (e.g. Grevesse & Sauval 1998) and for our best-fit solar model we obtained $A(\text{Li}) = 1.04$. We also checked that the sound velocity profile of our best-fit model is consistent with that deduced from helioseismology inversions by Basu et al. (1997). Our calibration is in an excellent agreement with helioseismology, more accurately than 1% for most of the star, except in the deep interior, where the discrepancy reaches 1.5%.

We computed a grid of evolutionary models of masses in the 0.90 to $1.34 M_{\odot}$ range, with a step of $0.01 M_{\odot}$ in mass, and with a metallicity of $[\text{Fe}/\text{H}] = 0.01$, which is a simple average of different estimates for the metallicity of M67 (see Pasquini et al. 2008). We run the models from the zero age main sequence (ZAMS) to the top of the red giant branch (RGB) for the most massive stars. The input parameters for all the models are the same as for the $1.00 M_{\odot}$ model.

There is no a priori reason why the calibration of the parameters of the extra mixing for the model of $1.00 M_{\odot}$ should hold also for different masses, and at different times during the evolution of the stars. In their work, Théado & Vauclair

(2003b) adjusted the free parameters of the rotation-induced mixing with the TGEC for each one of the models of different masses to obtain the correct lithium depletion at the age of the Hyades. They noted that the horizontal diffusion coefficient is very mass-dependent. The uncertainty associated to these parameters led us to analyze their impact on the destruction of lithium as a function of stellar mass. To do so, a first set of models is calculated to reproduce the profile of lithium abundance as a function of mass for the Hyades open cluster. Our Hyades sample is a compilation of EW measurements of the lithium line at 6708 Å from several sources (Randich et al. 2007; Thorburn et al. 1993; Soderblom et al. 1990; Boesgaard & Budge 1988; Boesgaard & Tripicco 1986; Duncan & Jones 1983; Rebolo & Beckman 1988). All the stars identified in Thorburn et al. (1993) as binaries were excluded. When more than one reference was available for a star, we used the most recent. Masses and temperatures were taken either directly from Balachandran (1995), or computed from the relationship between B-V and, respectively, mass and temperature, obtained from the data in the same paper. The result of the compilation is available at CDS in electronic form (Table 2). The parameters C_h and α_{turb} of the rotation-induced mixing of the models, with masses from 0.800 to $1.400 M_{\odot}$, with a step of $0.050 M_{\odot}$, are calibrated to reproduce at the age of the Hyades (625 Myr) the observed destruction of lithium. In these calibrations, we did not include the tachocline which is used in the code to calibrate solar models, related to the fact that in the solar mass stars the bottom of the convective zone is very close to the lithium destruction layer (Théado & Vauclair 2003b). The same calibration is then used to calculate a set of models of M67 stars. The values of the parameters C_h and α_{turb} for all calibrations are given in Table 4.

5. Discussion

Some amount of spread in the lithium abundance versus mass distribution observed in M67 for stars of about one solar mass or lower, **which can be clearly seen in Fig. 2**, suggests that an extra variable (besides mass, age and metallicity) is at work, leading to different lithium depletion in cluster stars of the same mass. The fundamental question here (since the spread is present) is what other variable may cause a large range of lithium abundance at a fixed mass?

Our database includes stars ranging from the main sequence to the sub-giant and giant branches, so it is well-suited both to address the issue of spread and to test models of non-standard mixing for different masses.

Models that point to rotational mixing as the major cause of lithium depletion (see e.g. Pinsonneault 2010, for a review), predict that this only depends on age, metallicity, mass, and the initial angular momentum of the star. This last parameter, however, may vary for otherwise similar stars, introducing a spread in lithium abundances. The variation of the initial rotation velocity by a factor 2 in our models have a weak influence, about 0.05 dex of magnitude for the lithium destruction, because the Skumanich's law used implies a strong drop of the rotation velocity very early in the star evolution. The Skumanich's law is empirical, and we should in the future include in the code the transport of angular momentum to have a better estimation of the spread of the lithium abundance due to a possible spread in the initial angular momentum.

The depth of the surface convection zone and the nuclear burning depend strongly on the total stellar mass (do Nascimento et al. 2009), thus, the appropriate way to inves-

Table 4. Parameters of the rotation-induced mixing in TGEC models.

Calibration	Mass (M_{\odot})	C_h	α_{turb}
Sun	1.000	9000	1.00
Hyades	0.800	3400	4.00
	0.850	10000	5.00
	0.900	10000	5.50
	0.950	10000	5.60
	1.000	10000	5.15
	1.050	7000	4.25
	1.100	5000	3.30
	1.150	4500	2.50
	1.200	2500	2.10
	1.250	2546	2.15
	1.300	2600	2.75
	1.350	6500	3.50
	1.400	10000	4.50

tigate the abundance of lithium in these M67 stars is first of all divide our sample of stars in three different group of mass range: MS stars with $M \leq 1.1 M_{\odot}$, stars close to the turnoff with $1.1 M_{\odot} < M \leq 1.28 M_{\odot}$, and evolved sub-giant and giant stars with $M > 1.28 M_{\odot}$.

5.1. Lithium abundance and mass

In Fig. 2 we compare the predictions of our models with our inferred stellar masses and lithium abundances for our sample of M67 stars. The solid line represents an isochrone constructed with all the models including the effects of atomic diffusion, gravitational settling and rotation-induced mixing calibrated on the Sun as described in Sect. 4. The age of the models is 3.87 Gyr as determined in Castro et al. (2011). Initial lithium abundances have been chosen equal to $A(\text{Li}) = 3.26$, the estimated initial solar value based on meteorites (Asplund et al. 2009). This lithium abundance is 0.05 dex lower than the previously accepted meteoritic lithium abundance ($A(\text{Li}) = 3.31$, see Grevesse & Sauval 1998). The dashed line represents an isochrone with the same models but where the initial lithium abundance was rescaled by -0.45 dex to fit the plateau at $A(\text{Li}) = 2.5$. This suggests that the initial M67 lithium abundance may have been lower than 3.26, or that our models are not depleting enough lithium. Note, however, that according to Deliyannis et al. (1994), based on a short-period tidally locked binary in M67, the initial lithium abundance in M67 was at least $A(\text{Li}) = 3.0$. This would reduce the shift necessary to match our models with the lithium content in the plateau to only about -0.2 dex. However, the hypothesis of a lower initial lithium content seems weak and not realistic. We are left with an insufficient destruction of lithium by rotationally-driven mixing mechanisms. Théado & Vauclair (2003b) showed that for masses larger than $1.0 M_{\odot}$, it is necessary to increase the values of these parameters as a function of mass to account for the lithium depletion at the age of the Hyades. To analyse the influence of these parameters on the lithium destruction, we calculated another set of models, with the rotation-induced mixing parameters calibrated for each mass, as described in Sect. 4. The isochrone at the age of M67 of these models is represented by the dotted line in Fig. 2. These models reproduce quantitatively better the profile of lithium destruction in M67, but the arbitrary calibration of mixing parameters for each mass is not a very satisfactory method. It appears no clear relation between the mixing parameters and mass that could have a physical significance.

For stars with masses below $1.1 M_{\odot}$ (roman number I in Fig. 1 and Fig. 2), the lithium depletion progressively increases

for lower masses. For masses below this threshold, the lithium depletion increases drastically with decreasing mass. A dispersion is observed in this mass range and is confirmed by several authors (Pasquini et al. 1997; Jones et al. 1999; Randich et al. 2002, 2007; Pasquini et al. 2008). It should be noted that in this region, some upper limits used may be considered too optimistic. On this regard, Önehag et al. (2011) analyzed the M67 solar twin YBP 1194 using spectra of good quality ($R \sim 50,000$, $S/N = 160$), but even with such a spectrum they found that it is challenging to determine a firm lithium abundance in the solar twin YBP 1194. A careful analysis of solar analogs in M67 using high quality spectra is urgently needed for stars around $1 M_{\odot}$. However, we note that four stars at $1.01 M_{\odot}$ span as a wide range of lithium abundances as 1.1 dex, and one of them is a revised upper limit. A considerable amount of scatter in the data in this region holds after raising the upper limits, and its real presence should be considered highly probable based on the presently available data. Stellar rotation and the history of angular momentum induce it either directly through rotational mixing or indirectly by driving other processes such as diffusion and internal gravity waves (Montalbán & Schatzman 2000). Planetary accretion may also be at work in solar-type stars, and induce mass-independent lithium destruction (Théado et al. 2010).

The low lithium abundance observed in low mass stars in M67 is also because these stars have more time to burn their lithium during the pre main sequence and have a surface convection zone which both retreats more slowly and ends up deeper on the main sequence. Notice that, for this range of masses and these evolutionary stages, the standard models predict that the bottom of the convective zone is not hot enough to account for the decrease of lithium, yet the observed low lithium abundances clearly indicates the need for a more realistic representation of transport mechanisms in low mass stars.

Stars with masses $1.1 M_{\odot} < M \leq 1.28 M_{\odot}$ (between roman number I and II in Fig. 1 and Fig. 2) are close to the turn off (or about to leave the main sequence) and at these masses the surface convection zone and the mixed layers below the convection zone are too thin to support temperatures high enough to cause nuclear destruction of lithium. On this range the pre main sequence lithium depletion tapers off to essentially zero. We can therefore easily see why there should be a plateau with nearly constant lithium abundance for this mass range. One important test of our model will be in fact to reproduce the general morphology of the lithium depletion behavior.

This is the region where the offset between our models and observations becomes apparent, as discussed above.

Stars with masses above $1.28 M_{\odot}$ are sub-giants following an evolutionary path from the turn-off to the red giant branch. In Fig. 1 and Fig. 2 this stage is marked by the roman numbers II and III. The lithium abundance predicted for standard models for sub-giant and giant stars is mainly controlled by dilution (Iben 1966, 1967a,b; Scalo & Miller 1980). This process was described originally by Iben (1965) and appears when a star evolves off the MS. When the star crosses the sub-giant branch and climbs the RGB, the surface convective zone increases its fraction in mass. Lithium poor material arises to the surface and is mixed with Li-rich material. This process stops when the convective zone achieves its maximum size. From our models the predicted value for lithium abundance post-dilution is $A(\text{Li}) = 1.0$ dex. The observations clearly show the need for a non-standard transport processes for sub-giants and evolved stars of M67. Recently, Canto Martins et al. (2011) discussed the depletion of the surface lithium abundance and whether there is a further non standard transport process related to transport of matter and angular momentum by meridional circulation and shear-induced turbulence (Ryan & Deliyannis 1995).

5.2. Prediction by other models

Our models successfully reproduce qualitatively the lithium depletion seen in different mass regimes in M67 stars, as shown in Fig. 2. In Fig. 3 the evolution with age at different masses is shown. It is important to notice that fully independent non-standard models by Xiong & Deng (2009), also show similar trends between lithium depletion, mass and age.

As shown in Fig. 1 of Xiong & Deng (2009), at 4 Gyr, there is a large depletion of lithium for models with $1 M_{\odot}$. As in our models, the less depleted stars are those with masses somewhat higher than $1.1 M_{\odot}$, yet the Xiong & Deng (2009) model also fails to predict exactly the peak or plateau in lithium abundance for M67 stars close to the turnoff, requiring probably an additional lithium depletion of 0.3 dex. Stars with masses higher than $1.3 M_{\odot}$ show severe depletion at 4 Gyr, probably because they should be in the sub-giant or giant phase. Thus, qualitatively, the models by Xiong & Deng (2009) also reproduce the M67 observations.

5.3. Deviant stars

Although overall lithium abundance appears to be a tight function of mass for stars more massive than $1.06 M_{\odot}$, a few objects dramatically depart from the general trend.

These objects are marked by open square symbols in Fig. 1 and Fig. 2, and are discussed below.

YBP 1075, YBP 750, YBP 769: These objects, despite being quite distant from the isochrone in the CMD diagram (more than 0.1 mag, limit under which 80% of the sample lies), are all secure members (99 or 100% of probability, based also on radial velocity). They are therefore likely to have companions too small to be detected, but bright enough to affect color and brightness. Their lithium abundance deficiency, with respect to the mean trend with the mass, is of about 2.3, 1.0, and 0.5 dex respectively, much more than errors can possibly explain, and they have estimated masses in the narrow range between 1.12 and $1.18 M_{\odot}$. Therefore the question whether we are facing a “secondary dip” is legitimate, although strong caution should be exercised before claiming it as highly probable. Their mass range encompasses 4 more stars, 3 of which lie significantly closer to the isochrone. If we formulate the intriguing hypothesis of an

extra-mixing mechanism triggered in this narrow mass range by a low mass companion, we are still left with the unexplained case of YBP 1680, which is also likely to have a small undetected companion, but does not show any anomaly as far as lithium abundance is concerned. The matter deserves further attention.

YBP 890: Also this star is a secure member, but, contrary to the 3 discussed above, its distance to the isochrone in the CMD is of only 0.03 mag. It has a mass of about $1.24 M_{\odot}$, and it has a lithium abundance about 0.9 dex lower than YBP 961, estimated to be at about the same mass. Its lithium abundance is an upper limit, it may therefore be more peculiar than it appears. This star has undoubtedly undergone a strong amount of extra mixing.

YBP 871 and YBP 778 are also significantly under-abundant in lithium, and have masses similar to that of YBP 890. Their distance to the isochrone in the CMD is of about 0.06 mag, larger than for YBP 890, but not dramatic. In their case, however, we still cannot completely rule out the possibility of a conspiracy of errors in the abundance and in the mass to explain their peculiar position in Fig. 2.

YBP 942: Is a secure member of the cluster, the only star with a peculiar high lithium abundance, which is 0.5 and 0.8 dex larger than the slightly less massive stars YBP 1320 and YBP 1318. Rather than an error in the abundance, an overestimation of the mass of this star of about $0.05 M_{\odot}$ could help to explain its abundance anomaly. However, its distance from the isochrone in the CMD is large but not outstanding, about 0.1 mag.

5.4. Lithium abundance, rotation and chromospheric activity in M67

In stars with a convective envelope, the chromosphere and chromospheric activity are generated by non-radiative heating mechanisms due to the presence of a magnetic field (see e.g. Hall 2008, for a review). Rotation and differential rotation play a key role in this process, because they are at the base of the dynamo effect that sustain magnetic activity (Böhm-Vitense 2007). Magnetic braking spins down the star, which therefore loses chromospheric activity as it loses angular momentum. While until a few years ago there was general consensus on the fact that chromospheric activity decays smoothly during the whole stellar life time (e.g. Skumanich 1972; Barry et al. 1987; Soderblom et al. 1991; Donahue 1998; Lachaume et al. 1999), which is still widely accepted (Mamajek & Hillenbrand 2008), alternative views have also been expressed later on (Pace et al. 2009; Lyra & Porto de Mello 2005; Zhao et al. 2011). However, nobody questions the fact that young stars are more chromospherically active than stars older than 1.5 Gyr (Soderblom 2010).

This picture suggests that chromospheric activity may be related to rotation and age, in a very similar way as lithium abundance is. This is the rationale for a comparison between these 3 parameters in M67.

The most extensive chromospheric-activity survey made in M67 is that by Giampapa et al. (2006), who collected data for over 60 main-sequence stars. They used the HK index, i.e. a measure of the strength of the chromospheric emission in the core of the Ca II H and K line, in mÅ. The HK index is neither transformed into flux, nor corrected for photospheric contribution. Mamajek & Hillenbrand (2008) transformed the HK indices of Giampapa et al. into R'_{HK} , i.e. they subtracted the photospheric contribution, they transformed it into flux, and they normalized it for the bolometric emission. The data were taken

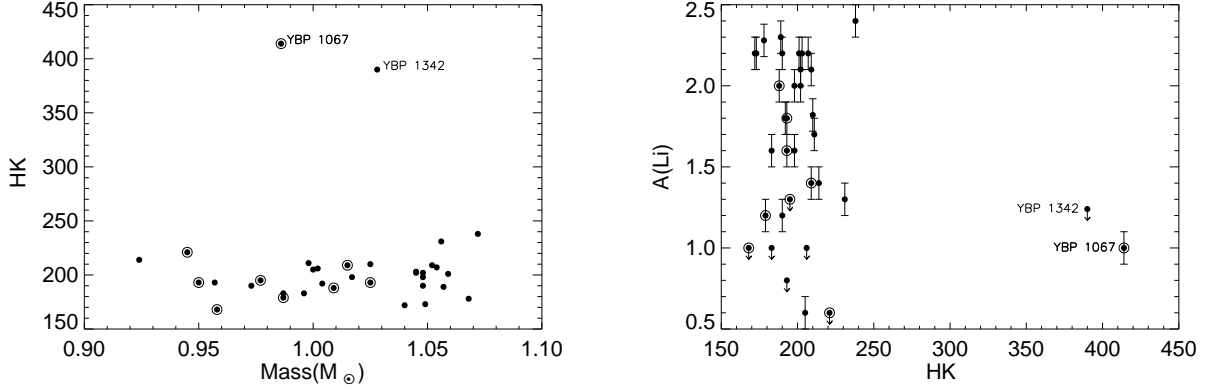


Fig. 4. On the left: chromospheric activity as a function of mass. On the right: lithium abundances versus chromospheric activity. Empty circles around filled symbols indicate the stars with measured projected rotation velocity. Among such measurements, only that of YBP1067 exceeds 2 km s^{-1} , and it is of 4 km s^{-1} .

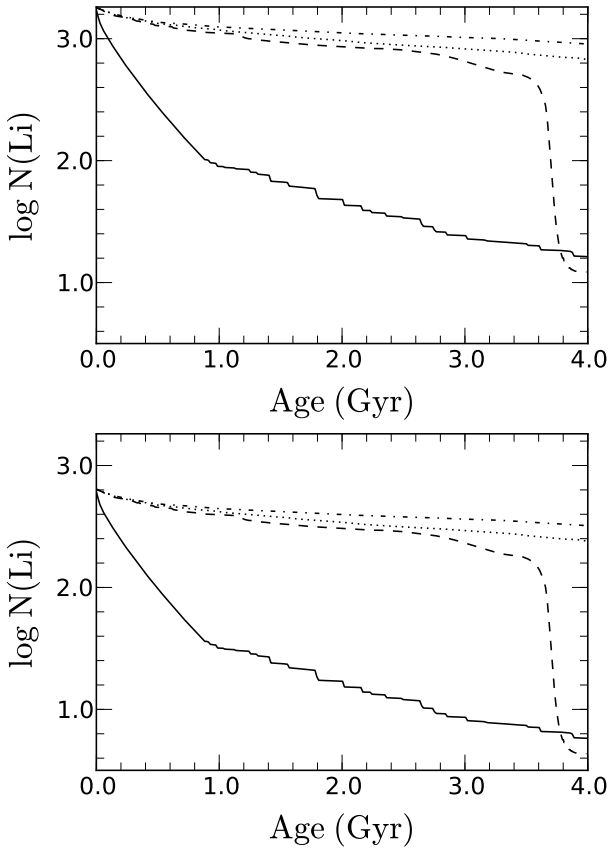


Fig. 3. Lithium abundance predicted by our models as a function of time for different masses. *Upper panel:* for a main sequence star with $M = 1 M_{\odot}$ (solid line), stars of $M = 1.15 M_{\odot}$ (dot-dashed) and $1.28 M_{\odot}$ (dotted) currently around the turn-off, and a more massive star of $1.33 M_{\odot}$ (dashed line) that is already a giant. *Lower panel:* same plot, but after a -0.45 dex shift was applied (as in Fig. 2).

over a time span of five years, and measurements for each star were time averaged over large part of this interval, which is of crucial importance since chromospheric activity has short term

variations analogs of the 11-year solar cycle. 35 stars studied by Giampapa et al. have published lithium abundances collected here, and they are plotted in Fig. 4. In this figure we show the HK index in $\text{m}\text{\AA}$ as a function of mass (*Left panel*) and HK index versus lithium abundances (*Right panel*). Here upper limits are indicated as downward arrows. Circles surrounding dots indicate that the star has a rotation velocity measurement available (see below). The left panel has the purpose of identifying the two active outliers. It is similar to Fig. 4 in Giampapa et al., in which B-V color is a substitute for mass, but notice that out of the two active stars in both figures only one is in common: Sanders1050/YBP1342. Sanders747/YBP681 is in Fig. 4 of Giampapa et al. and not in our Fig. 4 because it is a binary, and we excluded it from our compilation. On the contrary we plot Sanders1452/YBP1067, which is outside the margins of Fig. 4 of Giampapa et al.. In the *Right panel*, we show that the two active outliers are highly lithium depleted. However, such high levels of lithium depletion are also found in many other inactive stars. The Pearson correlation coefficient between the HK index and the lithium abundance is weak but significantly different from 0: -0.25 . Such weak correlation cannot be an effect of a correlation between HK index and mass, which, for our sample, are completely unrelated. However, the correlation between HK index and lithium abundance is entirely due to the two chromospherically-active and highly-lithium depleted stars. If we remove them, the correlation between HK and lithium abundance is -0.05 , which corresponds to a probability of the two quantities being unrelated of about 80%.

Reiners & Giampapa (2009) measured projected rotation velocity of 15 stars selected from the sample of Giampapa et al. in order to check whether rotation was at the base of the higher chromospheric activity level of some stars. The measurement were based on the cross correlation profile of high-resolution spectra. Nine of these stars are present in our compilation of lithium abundances, and they are indicated in Fig. 4 with a circle surrounding the dot. With the only exception of YBP1067, all of the projected rotation velocities are consistent with the solar rotation, as they have an upper limit of about 2 km s^{-1} . YBP1067, on the contrary, has a projected rotation velocity of about 4 km s^{-1} , i.e. it rotates at least twice as faster as the sun. Whether this suggests a relationship between rotation and lithium abundance or not, is not clear. On the one hand, YBP1067 has a very low lithium abundance, on the other hand there are two slow rotators with an even lower lithium content and one more slow

rotator with an upper limit only slightly above the lithium abundance measurement for YBP1067. More data are warranted to shed light on this matter. In particular, it would be very important to obtain true rotation periods instead of only $v \sin i$.

6. Conclusions

M67 provides important constraints to test non-standard models of lithium depletion. We have re-derived the effective temperatures of M67 stars and corrected the lithium abundances available in the literature, in order to have a homogeneous data-set for comparison with our models. We have also taken into account NLTE effects, providing a homogeneous set of NLTE Li abundances in M67. Tables with our T_{eff} , NLTE lithium abundances and masses are presented, so that other groups can test their non-standard stellar models.

M67 stars close to the turn-off, with masses $M = 1.1 - 1.28 M_{\odot}$, have a peak or a plateau in lithium abundances. Less massive stars ($M < 1.1 M_{\odot}$) show strong lithium depletion, which increases for lower masses due to a deepening of their convection zones. Evolved sub-giant and giant stars with $M > 1.28 M_{\odot}$ show lower Li abundances due to a dilution of their original lithium content. The above pattern is qualitatively well-reproduced by our models, as well as by the independent models of Xiong & Deng (2009).

The lithium abundance appears to be a tight function of the mass, for stars more massive than the sun, with a few notable exceptions that deserve a closer look. In particular, based on 3 over-depleted stars, we suggest that, at about $1.15 M_{\odot}$, the presence of a small companion may trigger a strong extra mixing, or perhaps the initial rotation velocity was higher in these stars. More observations are needed before drawing firm conclusions on these outliers.

Our models qualitatively reproduce many observed features of the lithium abundance as a function of mass. However we are still far from a close match between observations and models with a unique combination of the parameters.

Two stars in our compilation have chromospheric activity levels unusually high. They are both highly lithium depleted but, apart of this circumstance, no strong relationship between chromospheric activity and lithium abundance seems to be present. Only for one of the two chromospherically active stars, projected rotation velocity was measured, and it is of $\sim 4 \text{ km s}^{-1}$, the only value that exceeds 2 km s^{-1} among 9 measurements in our sample. This suggests that rotation is at the base of both lithium depletion and higher chromospheric activity in this star, but other extra mixing processes must be at least as efficient in some slow rotators.

Acknowledgements. Valuable comments made by the referee helped to improve the quality of this paper. This research made use of the SIMBAD database, operated at CDS, Strasbourg, France, and of WEBDA, an open cluster database developed and maintained by Jean-Claude Mermilliod. The authors are grateful for the support from FCT/CAPES cooperation agreement n°237/09. G.P. is supported by grant SFRH/BPD/39254/2007 and by the project PTDC/CTE-AST/098528/2008, funded by Fundação para a Ciência e a Tecnologia (FCT), Portugal. Research activities of the Stellar Board at the Federal University of Rio Grande do Norte are supported by continuous grants from CNPq and FAPERN Brazilian Agencies. J.M. would like to acknowledge support from USP, FAPESP (2010/17510-3). J.D.N. and J.M. would like to acknowledge support from CNPq (Bolsa de Produtividade).

References

Alexander, D. R., & Ferguson, J. W. 1994, *ApJ*, 437, 879
Angulo, C., Arnould, M., Rayet, M., et al. 1999, *Nuclear Physics A*, 656, 3

Anthony-Twarog, B. J., Deliyannis, C. P., Twarog, B. A., Croxall, K. V., & Cummings, J. D. 2009, *AJ*, 138, 1171
Asplund, M., Grevesse, N., Sauval, A. J., & Scott, P. 2009, *ARA&A*, 47, 481
Bahcall, J. N., & Pinsonneault, M. H. 1992, *Reviews of Modern Physics*, 64, 885
Balachandran, S. 1995, *ApJ*, 446, 203
Barry, D. C., Cromwell, R. H., & Hege, E. K. 1987, *ApJ*, 315, 264
Basu, S., Christensen-Dalsgaard, J., Chaplin, W.J., Elsworth, Y., Isaak, G.R., New, R., Shou, J., Thompson, M.J., Tomczyk, S. 1997, *MNRAS*, 292, 243
Baumann, P., Ramírez, I., Meléndez, J., Asplund, M., Lind, K. 2010, *A&A*, 519, 87
Boesgaard, A. M., & Tripicco, M. J. 1986, *ApJ*, 302, L49
Boesgaard, A. M., & Budge, K. G. 1988, *ApJ*, 332, 410
Brun, A.S., Turck-Chièze, S., Zahn, J.-P. 1998, in *Structure and Dynamics of the Interior of the Sun and Sun-like Stars* ESA Publications Division, SP-418, 439
Brun, A.S., Turck-Chièze, S., Zahn, J.-P. 1999, *ApJ*, 525, 1032
Böhm-Vitense, E. 1958, *ZAp*, 46, 108
Böhm-Vitense, E. 2007, *ApJ*, 657, 486
Bouvier, J. 2008, *A&A*, 489, L53
Caffau, E., Maiorca, E., Bonifacio, P., Faraggiana, R., Steffen, M., Ludwig, H.-G., Kamp, I., Busso, M. 2009, *A&A*, 498, 877
Canto Martins, B. L., Lèbre, A., Palacios, A., de Laverny, P., Richard, O., Melo, C. H. F., Do Nascimento, J. D., Jr., & de Medeiros, J. R. 2011, *A&A*, 527, A94
Casagrande, L., Ramírez, I., Meléndez, J., Bessel, M., Asplund, M. 2010, *A&A*, 512, 54
Castro, M., Vauclair, S., & Richard, O. 2007, *A&A*, 463, 755
Castro, M., Do Nascimento, J. D., Jr., Biazzo, K., Meléndez, J., & de Medeiros, J. R. 2011, *A&A*, 526, A17
Chaboyer, B., Demarque, P., & Pinsonneault, M. H. 1995, *ApJ*, 441, 865
Charbonnel, C., Vauclair, S., & Zahn, J.-P. 1992, *A&A*, 255, 191
Charbonnel, C. & Talon, S. 1999, *A&A*, 351, 635
Charbonnel, C. & Talon, S. 2005, *Science*, 309, 2189
Chen, Y. Q., Nissen, P. E., Benoni, T., & Zhao, G. 2001, *A&A*, 371, 943
D'Antona, F., & Mazzitelli, I. 1984, *A&A*, 138, 431
D'Antona, F., & Mazzitelli, I. 1994, *ApJS*, 90, 467
D'Antona, F., & Montalbán, J. 2003, *A&A*, 412, 213
Delahaye, F., Pinsonneault, M. H. 2005, *ApJ*, 649, 529
Deliyannis, C. P., King, J. R., Boesgaard, A. M., & Ryan, S. G. 1994, *ApJ*, 434, L71
do Nascimento, J.-D., Jr., Charbonnel, C., Lebre, A., de Laverny, P., De Medeiros, J. R., 2000, *A&A*, 357, 931
do Nascimento, J.-D., Jr., Castro, M., Meléndez, J., Bazot, M., Théado, S., Porto de Mello, G. F., De Medeiros, J. R. 2009, *A&A*, 501, 687
Donahue, R. A. 1998, *Cool Stars, Stellar Systems, and the Sun*, 154, 1235
Duncan, D. K., & Jones, B. F. 1983, *ApJ*, 271, 663
Gaipe, Y. 1993, *A&A*, 269, 267
García Lopez, R. J., Rebolo, R., & Beckman, J. E. 1988, *PASP*, 100, 1489
Ghezzi, L., Cunha, K., Smith, V. V., & de la Reza, R. 2010, *ApJ*, 724, 154
Giampapa, M. S., Hall, J. C., Radick, R. R., & Baliunas, S. L. 2006, *ApJ*, 651, 444
Gonzalez, G. 2008, *MNRAS*, 386, 928
Gough, D., McIntyre, M.E. 1998, *Nature*, 394, 755
Grevesse, N., Noels, A. 1993, in *Origin and evolution of the elements: proceedings of a symposium in honour of H. Reeves, Paris, June 22-25, 1992*, by N. Prantzos, E. Vangioni-Flam and M. Casse. (eds), Cambridge University Press (Cambridge, England), p.14
Grevesse, N. & Sauval, A. J. 1998, *Space Sci. Rev.*, 85, 161
Guzik, J. A., & Mussack, K. 2010, *ApJ*, 713, 1108
Hall, J. C. 2008, *Living Reviews in Solar Physics*, 5, 2
Hobbs, L. M., & Pilachowski, C. 1986, *ApJ*, 311, L37
Hobbs, L. M., Iben, I., Jr., & Pilachowski, C. 1989, *ApJ*, 347, 817
Hui-Bon-Hoa, A. 2008, *Ap&SS*, 316, 55
Iben, I., Jr. 1965, *ApJ*, 142, 1447
Iben, I., Jr. 1966, *ApJ*, 143, 483
Iben, I., Jr. 1967, *ApJ*, 147, 624
Iben, I., Jr. 1967, *ApJ*, 147, 650
Iglesias, C.A., Rogers, F.J. 1996, *ApJ*, 464, 943
Israelian, G., et al. 2009, *Nature*, 462, 189
Jones, B. F., Fischer, D., Shetrone, M., & Soderblom, D. R. 1997, *AJ*, 114, 352
Jones, B. F., Fischer, D., & Soderblom, D. R. 1999, *AJ*, 117, 330
King, J. R., Krishnamurthi, A., & Pinsonneault, M. H. 2000, *AJ*, 119, 859
Kučinskas, A., Hauschildt, P. H., Ludwig, H.-G., Brott, I., Vansévičius, V., Lindegren, L., Tanabé, T., & Allard, F. 2005, *A&A*, 442, 281
Lambert, D. L., & Reddy, B. E. 2004, *MNRAS*, 349, 757
Lachaume, R., Dominik, C., Lanz, T., & Habing, H. J. 1999, *A&A*, 348, 897
Lind, K., Asplund, M., & Barklem, P. S. 2009, *A&A*, 503, 541
Lyra, W., & Porto de Mello, G. F. 2005, *A&A*, 431, 329

- Maeder, A., Zahn, J.-P. 1998, *A&A*, 334, 1000
- Mamajek, E. E., & Hillenbrand, L. A. 2008, *ApJ*, 687, 1264
- Meléndez, J., Asplund, M., Gustafsson, B., & Yong, D. 2009, *ApJ*, 704, L66
- Meléndez, J., Ramírez, I., Asplund, M., & Baumann, P. 2010, *IAU Symposium*, 268, 341
- Montalbán, J., & Schatzman, E. 1996, *A&A*, 305, 513
- Montalbán, J., & Schatzman, E. 2000, *A&A*, 354, 943
- Önehag, A., Korn, A., Gustafsson, B., Stempels, E., & Vandenberg, D. A. 2011, *A&A*, 528, A85
- Pace, G., Pasquini, L., & François, P. 2008, *A&A*, 489, 403
- Pace, G., Meléndez, J., Pasquini, L., Carraro, G., Danziger, J., François, P., Matteucci, F., & Santos, N. C. 2009, *A&A*, 499, L9
- Palacios, A., Talon, S., Charbonnel, C., Forestini, M. 2003, *A&A*, 399, 603
- Paquette, C., Pelletier, C., Fontaine, G., Michaud, G. 1986, *ApJS*, 61, 177
- Pasquini, L., Liu, Q., & Pallavicini, R. 1994, *A&A*, 287, 191
- Pasquini, L., Randich, S., & Pallavicini, R. 1997, *A&A*, 325, 535
- Pasquini, L., Biazzo, K., Bonifacio, P., Randich, S., Bedin, L. R. 2008, *A&A*, 489, 677
- Piau, L., & Turck-Chièze, S. 2002, *ApJ*, 566, 419
- Pietrinfermi, A., Cassisi, S., Salaris, M., & Castelli, F. 2004, *ApJ*, 612, 168
- Pinsonneault, M. H., Kawaler, S. D., Sofia, S., & Demarque, P. 1989, *ApJ*, 338, 424
- Pinsonneault, M. H. 2010, *IAU Symposium*, 268, 375
- Randich, S., Primas, F., Pasquini, L., & Pallavicini, R. 2002, *A&A*, 387, 222
- Randich, S., Sestito, P., & Pallavicini, R. 2003, *A&A*, 399, 133
- Randich, S., Sestito, P., Primas, F., Pallavicini, R., & Pasquini, L. 2006, *A&A*, 450, 557
- Randich, S., Primas, F., Pasquini, L., Sestito, P., & Pallavicini, R. 2007, *A&A*, 469, 163
- Randich, S., Pace, G., Pastori, L., & Bragaglia, A. 2009, *A&A*, 496, 441
- Rebolo, R., & Beckman, J. E. 1988, *A&A*, 201, 267
- Reiners, A., & Giampapa, M. S. 2009, *ApJ*, 707, 852
- Richard, O., Vauclair, S., Charbonnel, C., Dziembowski, W. A. 1996, *A&A*, 312, 1000
- Richard, O., Théado, S., Vauclair, S. 2004, *SoPh*, 220, 243
- Rogers, F. J., Nayfonov, A. 2002, *ApJ*, 576, 1064
- Ryan, S. G., & Deliyannis, C. P. 1995, *ApJ*, 453, 819
- Scalo, J. M., & Miller, G. E. 1980, *ApJ*, 239, 953
- Serenelli, A. M., Basu, S., Ferguson, J. W., & Asplund, M. 2009, *ApJ*, 705, L123
- Sestito, P., & Randich, S. 2005, *A&A*, 442, 615
- Sestito, P., Randich, S., & Pallavicini, R. 2004, *A&A*, 426, 809
- Sestito, P., Degl'Innocenti, S., Prada Moroni, P. G., & Randich, S. 2006, *A&A*, 454, 311
- Skumanich, A. 1972, *ApJ*, 171, 565
- Soderblom, D. R., Oey, M. S., Johnson, D. R. H., & Stone, R. P. S. 1990, *AJ*, 99, 595
- Soderblom, D. R., Duncan, D. K., & Johnson, D. R. H. 1991, *ApJ*, 375, 722
- Soderblom, D. R., Jones, B. F., Balachandran, S., et al. 1993a, *AJ*, 106, 1059
- Soderblom, D. R., Fedele, S. B., Jones, B. F., Stauffer, J. R., & Prosser, C. F. 1993b, *AJ*, 106, 1080
- Soderblom, D. R. 2010, *ARA&A*, 48, 581
- Spiegel, E. A., Zahn, J.-P. 1992, *A&A*, 265, 106
- Spite, F., Spite, M., Peterson, R. C., & Chaffee, F. H., Jr. 1987, *A&A*, 171, L8
- Takeda, Y., & Kawanomoto, S. 2005, *PASJ*, 57, 45
- Talon, S., Charbonnel, C. 1998, *A&A*, 335, 959
- Talon, S., Charbonnel, C. 2005, *A&A*, 440, 981
- Talon, S. 2008, *EAS Publications Series*, 32, 81
- Tautvaišiene, G., Edvardsson, B., Tuominen, I., & Ilyin, I. 2000, *A&A*, 360, 499
- Théado, S., Vauclair, S. 2003, *ApJ*, 587, 784
- Théado, S., Vauclair, S. 2003, *ApJ*, 587, 795
- Théado, S., Bohun, E., & Vauclair, S. 2010, *IAU Symposium*, 268, 427
- Thorburn, J. A., Hobbs, L. M., Deliyannis, C. P., & Pinsonneault, M. H. 1993, *ApJ*, 415, 150
- Turcotte, S., Richer, J., Michaud, G., Iglesias, C. A., Rogers, F. J. 1998, *ApJ*, 504, 539
- Vandenberg, D. A., Gustafsson, B., Edvardsson, B., Eriksson, K., & Ferguson, J. 2007, *ApJ*, 666, L105
- Vandenberg, D. A., Edvardsson, B., Eriksson, K., Gustafsson, B. 2008, *ApJ*, 675, 746
- Ventura, P., Zeppleri, A., Mazzitelli, I., & D'Antona, F. 1998, *A&A*, 331, 1011
- Xiong, D.-R., & Deng, L. 2005, *ApJ*, 622, 620
- Xiong, D.-R., & Deng, L.-C. 2006, *Chinese Astron. Astrophys.*, 30, 24
- Xiong, D. R. & Deng, L. 2009, *MNRAS*, 395, 2013
- Yadav, R. K. S., Bedin, L. R., Piotto, G., Anderson, J., Cassisi, S., Villanova, S., Platais, I., Pasquini, L., Momany, Y., Sagar, R. 2008, *A&A*, 484, 609
- Zahn, J.-P. 1992, *A&A*, 265, 115
- Zhao, J. K., Oswalt, T. D., Rudkin, M., Zhao, G., & Chen, Y. Q. 2011, *AJ*, 141, 107

Table 1. M67 data

ID	RA	dec	V (mag)	B-V (mag)	mem. prob.	v_{rad} (km s ⁻¹)	A(Li) (dex)	ref	ph	T_{effref} (K)	T_{effiso} (K)	T_{effcal} (K)
Sand 774	132.70804	11.82025	12.930	0.850	-	33.500*	≤ 0.00	1	2	5240	5318	5253
YBP 1632	132.75075	11.90892	12.734	0.795	100	33.400	0.00 ± 0.20	1	1	5461	5514	5358
Sand 978	132.82283	11.75631	9.720	1.370	-	34.700*	-1.00 ± 0.30	1	2	4260	4311	4283
YBP 1087	132.84502	11.80048	10.413	1.139	98	33.900	≤ 0.00	1	1	4748	4560	4673
Sand 1016	132.82129	11.80453	10.300	1.260	-	34.600*	-0.50 ± 0.20	1	2	4430	4504	4432
YBP 1248	132.82726	11.82263	12.639	0.615	99	34.600	1.30 ± 0.10	1	1	6020	5753	5953
YBP 1479	132.80289	11.87846	10.462	1.127	97	34.200	-0.40 ± 0.20	1	1	4750	4593	4655
YBP 829	132.87231	11.75768	12.891	0.935	100	32.900	≤ 0.10	1	1	5130	5082	5070
YBP 923	132.93336	11.77347	12.753	0.744	100	32.719	≤ 0.80	1	1	5644	5550	5495
YBP 942	132.90004	11.77599	12.678	0.723	99	37.972	2.70 ± 0.10	1	1	5810	5620	5730
YBP 973	132.93642	11.77945	12.944	0.904	99	33.009	0.00 ± 0.20	1	1	5170	5082	5070
YBP 1060	132.93782	11.79609	11.465	1.040	97	32.900	≤ -0.40	1	1	4820	4820	4782
YBP 1258	132.95813	11.82532	12.616	0.587	99	32.700	0.90 ± 0.10	1	1	5996	6152	6054
YBP 1318	132.91347	11.83439	12.238	0.572	98	34.641	1.90 ± 0.10	1	1	6159	5991	6089
YBP 1320	132.90587	11.83479	12.579	0.606	99	34.322	2.20 ± 0.10	1	1	6050	5956	6020
YBP 1327	132.92642	11.83545	11.598	1.057	98	34.600	≤ -0.40	1	1	4820	4842	4782
YBP 1362	132.87080	11.84253	10.492	1.122	97	33.650	-0.50 ± 0.20	1	1	4779	4581	4655
YBP 1546	132.89908	11.89299	12.245	0.986	96	33.978	≤ -0.20	1	1	4940	4939	4901
YBP 1777	132.95349	11.94757	12.870	0.932	99	34.400	≤ 0.40	1	1	5104	5068	4944
YBP 1844	132.89752	11.96571	12.764	0.736	91	33.200	≤ 1.00	1	1	5654	5459	5439
YBP 846	133.04730	11.76054	12.838	0.824	100	33.100	≤ 0.00	1	1	5420	5386	5331
YBP 1876	133.01979	11.97474	12.577	0.641	99	33.921	1.10 ± 0.10	1	1	5940	5753	5856
Sand 1607	133.08937	11.84492	12.620	0.560	-	33.700*	1.70 ± 0.10	1	2	6127	6122	6124
YBP 1070	132.88519	11.79788	12.631	0.620	100	33.637	1.20 ± 0.10	1	1	6000	5753	5920
YBP 1086	132.88501	11.80033	12.752	0.821	100	33.000	0.70 ± 0.10	1	1	5429	5496	5331
YBP 285	132.84946	11.64782	14.461	0.704	98	33.951	0.60 ± 0.10	2	1	5836	5803	5657
YBP 637	132.84099	11.72159	14.489	0.702	99	34.241	1.50 ± 0.10	2	1	5806	5793	5663
YBP 1101	133.03522	11.80291	14.675	0.702	99	32.927	≤ 0.60	2	1	5756	5696	5663
YBP 1194	132.75336	11.81466	14.614	0.667	99	33.673	≤ 1.30	2	1	5766	5730	5770
YBP 1303	132.73610	11.83184	14.641	0.677	99	33.241	1.20 ± 0.10	2	1	5716	5707	5739
YBP 1304	132.85852	11.83208	14.731	0.723	99	33.696	≤ 0.80	2	1	5704	5662	5601
YBP 1315	132.99490	11.83403	14.297	0.693	99	32.434	1.80 ± 0.10	2	1	5874	5880	5691
YBP 1392	132.74921	11.85350	14.811	0.716	97	34.171	≤ 0.60	2	1	5716	5615	5622
YBP 1787	132.78810	11.95010	14.547	0.667	98	33.386	1.60 ± 0.10	2	1	5768	5763	5770
YBP 2018	132.91422	12.01588	14.565	0.672	98	31.740	≤ 1.30	2	1	5693	5752	5755
YBP 266	132.86034	11.64358	13.601	0.611	100	33.392	2.50 ± 0.10	3	1	6147	6144	5950
YBP 288	132.90065	11.64898	13.857	0.637	99	32.796	2.30 ± 0.10	3	1	6004	6077	5865
YBP 349	132.97981	11.66116	14.301	0.677	93	34.132	≤ 1.00	3	1	5952	5880	5739
YBP 350	132.83662	11.66115	13.624	0.602	99	32.778	2.60 ± 0.10	3	1	6024	6139	5980
YBP 401	132.82935	11.67103	13.661	0.607	97	32.917	2.40 ± 0.10	3	1	6165	6130	5963
YBP 473	132.80974	11.68589	14.443	0.699	99	35.269	≤ 1.00	3	1	5919	5812	5672
YBP 587	132.91141	11.71039	14.107	0.646	99	33.265	2.30 ± 0.10	3	1	6077	5972	5836
YBP 613	132.82542	11.71520	13.254	0.653	99	33.274	2.60 ± 0.10	3	1	6202	6134	5814
YBP 673	132.72226	11.72779	14.356	0.706	99	32.902	1.40 ± 0.10	3	1	5639	5851	5652
YBP 689	132.87555	11.73052	13.120	0.663	99	33.461	2.30 ± 0.10	3	1	6093	6169	5783
YBP 750	132.72267	11.74296	13.576	0.639	100	33.709	1.50 ± 0.10	3	1	5918	6148	5859
YBP 769	132.95924	11.74918	13.478	0.641	100	34.414	2.00 ± 0.10	3	1	5984	6162	5852
YBP 778	132.83669	11.75068	13.093	0.623	99	33.815	1.70 ± 0.10	3	1	6114	6169	5911
YBP 809	132.75854	11.75531	14.959	0.737	97	32.948	≤ 1.00	3	1	5667	5533	5561
YBP 851	132.85413	11.76193	14.113	0.617	98	34.204	1.30 ± 0.10	3	1	5948	5972	5930
YBP 911	132.79131	11.77137	14.547	0.673	99	32.534	1.20 ± 0.10	3	1	5885	5763	5752
YBP 988	132.89217	11.78216	14.180	0.639	99	32.705	2.00 ± 0.10	3	1	5935	5936	5859
YBP 1032	132.98578	11.79027	14.358	0.639	97	34.302	1.60 ± 0.10	3	1	5955	5851	5859
YBP 1036	132.85124	11.79121	14.947	0.731	98	33.884	1.40 ± 0.10	3	1	5612	5545	5578
YBP 1051	132.92290	11.79337	14.090	0.636	99	32.029	2.20 ± 0.10	3	1	6081	5981	5868
YBP 1062	132.90031	11.79639	14.477	0.667	99	33.206	1.70 ± 0.10	3	1	5926	5793	5770
YBP 1067	133.01459	11.79669	14.559	0.642	100	34.670	1.00 ± 0.10	3	1	5929	5763	5849
YBP 1075	132.91272	11.79871	13.712	0.674	99	32.974	0.70 ± 0.10	3	1	5871	6117	5749
YBP 1088	132.95395	11.80060	14.492	0.659	93	33.199	≤ 1.00	3	1	5890	5793	5795

Continued on next page

Table 1 – continued from previous page

ID	RA	dec	V (mag)	B-V (mag)	mem. prob.	v_{rad} (km s ⁻¹)	A(Li) (dex)	ref	ph	T_{effref} (K)	T_{effiso} (K)	T_{effcal} (K)
YBP 1090	132.86957	11.80061	13.800	0.650	100	32.333	2.30 ± 0.10	3	1	6086	6094	5824
YBP 1129	132.88573	11.80669	14.171	0.624	99	34.528	2.10 ± 0.10	3	1	5959	5945	5907
YBP 1137	132.80011	11.80741	14.873	0.698	97	33.851	≤ 1.00	3	1	5741	5592	5675
YBP 1197	132.87737	11.81522	13.315	0.606	100	34.526	2.20 ± 0.10	3	1	6207	6148	5967
YBP 1247	132.81271	11.82252	14.144	0.609	99	32.991	2.10 ± 0.10	3	1	5994	5954	5957
YBP 1334	132.86646	11.83664	14.403	0.680	99	32.923	2.00 ± 0.10	3	1	5957	5832	5730
YBP 1387	132.87485	11.85250	14.098	0.626	99	33.828	2.30 ± 0.10	3	1	6090	5972	5901
YBP 1458	132.76248	11.87381	14.977	0.739	98	33.351	≤ 1.00	3	1	5640	5533	5555
YBP 1496	132.78133	11.88226	13.879	0.607	100	34.607	2.60 ± 0.10	3	1	6173	6072	5963
YBP 1504	132.86456	11.88403	14.171	0.625	99	33.733	2.20 ± 0.10	3	1	5934	5945	5904
YBP 1514	132.75317	11.88653	14.777	0.721	98	33.878	1.60 ± 0.10	3	1	5613	5639	5607
YBP 1587	132.84644	11.90139	14.163	0.641	99	32.336	2.00 ± 0.10	3	1	5975	5945	5852
YBP 1622	132.80121	11.90639	14.156	0.632	99	33.407	2.20 ± 0.10	3	1	6043	5945	5881
YBP 1716	132.86621	11.92804	13.299	0.619	96	33.948	2.30 ± 0.10	3	1	6030	6142	5924
YBP 1722	132.82802	11.93048	14.130	0.601	96	34.007	2.20 ± 0.10	3	1	6007	5963	5983
YBP 1735	133.00172	11.93529	14.332	0.661	97	33.104	0.90 ± 0.10	3	1	5959	5861	5789
YBP 1758	132.74683	11.94357	13.207	0.653	98	34.398	2.40 ± 0.10	3	1	6221	6134	5814
YBP 1768	132.90657	11.94572	14.404	0.656	99	34.222	2.10 ± 0.10	3	1	5844	5832	5805
YBP 1788	132.80411	11.95025	14.441	0.663	84	33.763	1.80 ± 0.10	3	1	5886	5812	5783
YBP 1852	133.01376	11.96795	13.962	0.613	99	32.324	2.10 ± 0.10	3	1	6009	6033	5943
YBP 1903	132.78316	11.98149	14.733	0.689	99	32.409	≤ 1.00	3	1	5609	5662	5703
YBP 1948	132.92831	11.99195	14.015	0.612	97	33.136	2.40 ± 0.10	3	1	6164	6016	5947
YBP 1955	132.74373	11.99430	14.212	0.630	98	32.588	2.20 ± 0.10	3	1	5961	5926	5888
YBP 901	132.78600	11.76994	13.422	0.554	100	-	2.63 ± 0.07	4	1	6191	6166	6106
YBP 963	132.83385	11.77825	12.760	0.565	100	-	2.10 ± 0.08	4	1	6210	6223	6120
Sand 998	132.82230	11.78350	13.060	0.558	-	-	2.64 ± 0.06	4	2	6223	6211	6131
YBP 871	132.83470	11.76457	13.152	0.582	100	-	1.86 ± 0.16	4	1	6156	6149	6075
Sand 1064	132.84100	11.86170	14.040	0.661	-	32.700*	2.14 ± 0.10	5	2	5845	5998	5789
YBP 713	132.84070	11.73473	14.172	0.714	99	35.443	2.07 ± 0.10	5	1	5800	5936	5755
YBP 1105	132.98558	11.80347	13.946	0.590	99	32.800	2.55 ± 0.10	5	1	6094	6033	5990
YBP 1397	132.88300	11.85462	14.009	0.622	97	36.808	2.28 ± 0.10	5	1	5972	6007	5891
YBP 1342	132.82610	11.83879	14.285	0.650	99	33.684	≤ 1.15	5	1	5810	5880	5761
Sand 1057	132.83400	11.85050	14.300	0.668	-	34.500*	1.75 ± 0.10	5	2	5818	5880	5767
YBP 1486	132.83400	11.88000	13.864	0.574	94	-	2.63 ± 0.10	6	1	6178	6081	6058
YBP 890	132.83563	11.76801	13.179	0.590	100	34.212	≤ 1.48	6	1	6153	6139	6041
YBP 961	132.84187	11.77804	13.190	0.576	100	34.590	2.37 ± 0.10	6	1	6151	6139	6037
YBP 1680	132.88359	11.91907	13.646	0.645	100	35.428	2.45 ± 0.10	6	1	5934	6120	5862
Sand 1055	132.78600	11.84810	13.800	0.593	-	-	2.43 ± 0.10	6	2	6116	6094	6010
ES 1017	132.78500	11.78690	12.400	0.990	-	-	≤ 0.50	7	2	4700	4961	4901

References:

- (1) Canto Martins et al., 2011, *A&A* 527, A94;
- (2) Castro et al., 2011, *A&A* 526, 17;
- (3) Pasquini et al., 2008, *A&A* 489, 677;
- (4) Randich et al. 2007, *A&A* 469, 163;
- (5) Jones, Fischer and Soderblom 1999, *ApJ* 117, 330, original data;
- (6) Jones, Fischer and Soderblom 1999, *ApJ* 117, 330, correction of literature measurements;
- (7) Hobbs and Pilachowski, 1986, *ApJ* 311, L37.

Table 2. Hyades data

vB	V	B-V	T_{eff}	log g	Mass	EW	ΔEW	A(Li)	ΔA	EW ref	phot ref
2	7.78	0.617	5916	4.36	1.140	89.0	2	2.73	0.03	T	Bal.
3	8.88	0.848	5099	4.48	0.847	≤ 25.0		≤ 1.37		D	Bal.
4	5.97	0.341	6897	3.99	1.524	≤ 3.0		≤ 1.79		T	Bal.
6	5.95	0.348	6861	3.96	1.513	54.8	3	3.10	0.04	BB	Joner
8	6.37	0.419	6544	4.02	1.411	≤ 4.0		≤ 1.69		BB	Bal.
10	7.85	0.589	6000	4.42	1.182	82.0	2	2.74	0.03	T	Bal.
13	6.62	0.420	6542	4.12	1.410	≤ 5.0		≤ 1.79		BT	Bal.
14	5.73	0.355	6825	3.87	1.502	65.0	3	3.18	0.04	BT	Bal.
15	8.09	0.658	5703	4.39	1.037	57.0	2	2.32	0.03	T	Bal.
17	8.46	0.696	5539	4.47	0.971	42.0	2	2.03	0.05	T	Bal.
18	8.06	0.638	5779	4.41	1.072	74.0	2	2.52	0.04	T	Bal.
19	7.14	0.512	6231	4.22	1.290	82.4	3	2.91	0.03	BB	Bal.
20	6.32	0.399	6624	4.03	1.438	87.6	3	3.21	0.03	BB	Bal.
21	9.15	0.816	5207	4.63	0.872	≤ 3.0		≤ 0.58		Ra	Bal.
26	8.63	0.743	5437	4.51	0.936	13.0	2	1.39	0.07	T	Bal.
27	8.46	0.715	5506	4.46	0.960	23.0	2	1.72	0.04	T	Bal.
31	7.47	0.566	6067	4.29	1.215	95.0	2	2.88	0.02	T	Bal.
36	6.80	0.441	6463	4.17	1.382	5.9	3	1.81	0.18	BT	Bal.
37	6.61	0.405	6600	4.14	1.430	10.3	3	2.14	0.12	BT	Bal.
38	5.72	0.320	7019	3.93	1.560	19.6	3	2.70	0.14	BT	Bal.
42	8.86	0.759	5414	4.59	0.929	11.0	2	1.30	0.08	T	Bal.
44	7.19	0.450	6433	4.31	1.371	20.4	3	2.34	0.07	BT	Bal.
46	9.11	0.867	5028	4.55	0.832	≤ 4.0		≤ 0.55		T	Bal.
48	7.14	0.521	6203	4.21	1.278	91.0	2	2.95	0.02	T	Bal.
51	6.97	0.443	6457	4.23	1.380	6.5	3	1.84	0.17	BT	Bal.
49	8.24	0.585	6012	4.58	1.188	57.0	2	2.55	0.03	T	Bal.
59	7.49	0.543	6136	4.33	1.248	82.0	2	2.84	0.03	T	Bal.
61	7.38	0.514	6224	4.32	1.287	110.8	3	3.08	0.03	BB	Bal.
64	8.12	0.657	5707	4.40	1.039	59.0	2	2.34	0.03	T	Bal.
65	7.42	0.535	6160	4.31	1.259	106.0	2	3.00	0.03	T	Bal.
66	7.51	0.555	6100	4.32	1.231	73.0	2	2.75	0.03	T	Bal.
73	7.84	0.609	5940	4.39	1.152	85.0	2	2.72	0.03	T	Bal.
77	7.05	0.500	6263	4.20	1.304	19.0	6	2.20	0.13	Re	Bal.
76	9.20	0.759	5392	4.72	0.922	16.0	2	1.45	0.06	T	Bal.
78	6.92	0.453	6422	4.20	1.367	32.6	3	2.56	0.05	BB	Bal.
79	8.93	0.827	5171	4.53	0.863	≤ 3.0		≤ 0.56		T	Joner
81	7.10	0.470	6365	4.25	1.345	15.6	3	2.18	0.08	BT	Bal.
85	6.51	0.426	6519	4.07	1.402	≤ 6.0		≤ 1.85		BB	Bal.
86	7.05	0.463	6388	4.24	1.354	20.7	3	2.32	0.07	BT	Bal.
87	8.58	0.743	5437	4.49	0.936	12.0	2	1.36	0.07	T	Bal.
88	7.75	0.554	6103	4.42	1.232	89.0	10	2.86	0.06	S	Joner
90	6.40	0.413	6568	4.05	1.419	≤ 3.0		≤ 1.58		BB	Bal.
92	8.66	0.741	5443	4.52	0.938	15.0	2	1.46	0.06	T	Bal.
93	9.40	0.883	4968	4.64	0.820	≤ 3.0		≤ 0.29		T	Bal.
94	6.62	0.431	6499	4.11	1.395	≤ 2.2		≤ 1.40		BT	Bal.
97	7.93	0.634	5793	4.36	1.079	84.0	2	2.60	0.05	T	Bal.
99	9.38	0.851	5090	4.68	0.845	4.0	2	0.59	0.13	T	Bal.
101	6.65	0.433	6493	4.12	1.393	≤ 3.0		≤ 1.53		BB	Bal.
105	7.53	0.575	6042	4.31	1.203	87.0	2	2.81	0.02	T	Bal.
109	9.40	0.817	5203	4.73	0.871	5.0	1	0.74	0.09	Ra	Bal.
116	9.01	0.821	5191	4.57	0.868	≤ 5.0		≤ 0.73		T	Bal.
118	7.74	0.580	6026	4.39	1.195	77.0	2	2.72	0.03	T	Bal.
127	8.92	0.710	5520	4.65	0.964	18.0	2	1.62	0.05	T	SIMBAD
153	8.91	0.859	5062	4.48	0.839	8.0	2	0.82	0.10	T	Bal.
121	7.29	0.504	6256	4.29	1.301	114.9	3	3.12	0.02	BT	Bal.
124	6.25	0.501	6261	3.88	1.303	9.0	3	1.86	0.13	BT	Joner
128	6.75	0.450	6433	4.14	1.371	14.0	3	2.17	0.09	BT	Bal.
180	9.10	0.853	5081	4.57	0.843	5.0	2	0.65	0.13	T	Bal.
187	8.60	0.776	5352	4.46	0.912	17.0	1	1.44	0.04	Ra	Joner

References on next page

Table 2 – Data in the previous page

References for EW measurements:

- (Ra) Randich et al. 2007, A&A, 469, 163;
- (T) Thorburn et al., 1993, ApJ, 415, 150;
- (S) Soderblom et al., 1990, AJ, 99, 595;
- (BB) Boesgaard & Budge, 1988, ApJ, 332, 410;
- (BT) Boesgaard & Tripicco, 1986, ApJ, 302, L49;
- (D) Duncan & Jones, 1983, ApJ, 271, 663;
- (Re) Rebolo & Beckman, 1988, A&A, 201, 267;

References for the photometry:

- (Bal.) Balachandran, 1995, ApJ, 446, 203;
- (Joner) Joner et al., 2006, AJ, 132, 111;